International Journal of Computational Methods
Vol. 15, No. 1 (2018) 1850029 (35 pages)

DOI: 10.1142/S0219876218500299





# Application of Smoothed Finite Element Method to Two-Dimensional Exterior Problems of Acoustic Radiation

Yingbin Chai[*,§], Zhixiong Gong[*,†,‡,¶], Wei Li[*,†,‡,‖], Tianyun Li[*,†,‡,**], Qifan Zhang[*,†,‡,††], Zhihong Zou[*,†,‡,‡‡] and Yangbin Sun[*,†,‡,§§]

[*]*School of Naval Architecture and Ocean Engineering*
*Huazhong University of Science and Technology*
*Wuhan, Hubei, 430074, P. R. China*

[†]*Hubei Key Laboratory of Naval*
*Architecture & Ocean Engineering Hydrodynamics*
*Huazhong University of Science and Technology (HUST)*
*Wuhan, Hubei 430074, P. R. China*

[‡]*Collaborative Innovation Center for Advanced Ship and*
*Deep-Sea Exploration (CISSE)*
*Shanghai 200240, P. R. China*
[§]*cybhust@hust.edu.cn*
[¶]*hustgzx@hust.edu.cn*
[‖]*hustliw@hust.edu.cn*
[**]*ltyz801@hust.edu.cn*
[††]*hustzqf@hust.edu.cn*
[‡‡]*zouzhihong@hust.edu.cn*
[§§]*smzm755@163.com*

Received 19 February 2017
Revised 4 August 2017
Accepted 14 August 2017
Published 26 September 2017

In this work, the smoothed finite element method using four-node quadrilateral elements (SFEM-Q4) is employed to resolve underwater acoustic radiation problems. The SFEM-Q4 can be regarded as a combination of the standard finite element method (FEM) and the gradient smoothing technique (GST) from the meshfree methods. In the SFEM-Q4, only the values of shape functions (not the derivatives) at the quadrature points are needed and the traditional requirement of coordinate transformation procedure is not necessary to implement the numerical integration. Consequently, no additional degrees of freedom are required as compared with the original FEM. In addition, the original "overly-stiff" FEM model for acoustic problems (governed by the Helmholtz equation) is properly softened due to the gradient smoothing operations implemented over the smoothing domains and the present SFEM-Q4 possesses a relatively appropriate stiffness of the continuous system. Therefore, the well-known numerical dispersion error

‖Corresponding author.

for Helmholtz equation is decreased significantly and very accurate numerical solutions can be obtained by using relatively coarse meshes. In order to truncate the unbounded domains and employ the domain-based numerical method to tackle the acoustic radiation in unbounded domains, the Dirichlet-to-Neumann (DtN) map is used to ensure that there are no spurious reflections from the far field. The numerical results from several numerical examples demonstrate that the present SFEM-Q4 is quite effective to handle acoustic radiation problems and can produce more accurate numerical results than the standard FEM.

*Keywords*: Helmholtz equation; acoustic radiation; unbounded domain; numerical methods; gradient smoothing technique (GST).



## 1. Introduction

The acoustic radiation from vibrating structures is often encountered in practice for engineering. In order to effectively control the noise from the vibrating engineering components and improve the end-user's comfort, the researchers have made a great effort to concern this topic during the past few decades. In general, the analytical solutions are only available for the structures with simple geometrical shapes. When it comes to realistic problems with complicated geometrical shapes, the analytical solutions will be almost impossible or extremely difficult to obtain. In these cases, we have to resort to the numerical techniques. Compared to several analytical or semi-analytical methods for acoustic radiation or acoustic scattering problems [Seybert *et al.* (1986); DiPerna and Stanton (1994); Gong *et al.* (2016b, 2017)], the numerical methods are not limited to the geometries of the objects and can be used to handle more practical problems with arbitrary geometrical shapes.

In recent years, with the fast development of the computer science, various numerical techniques have been proposed to handle the acoustic radiation from an arbitrary body. Among them, the classical boundary element method (BEM) [Seybert *et al.* (1988)] and finite element method (FEM) [Assaad *et al.* (1993); Thompson (2006)] are two most powerful and versatile numerical approaches to tackle the acoustic problems. For the acoustic problems in the unbounded domains (such as the acoustic scattering or acoustic radiation), the classical BEM has several obvious advantages over the conventional FEM. As a typical boundary-based numerical technique, only the boundary discretization is required (this is quite different from the standard FEM) and the dimensions of the problem can be reduced to one in BEM. As a consequence, the number of system equations to be solved in BEM model is much less than that in FEM model. In addition, another superiority of the BEM for the problems in the unbounded domains is that the far field radiation condition (the Sommerfeld radiation condition) can be satisfied automatically and no special treatments are needed. Nevertheless, the BEM still suffers from few drawbacks: the system matrices generated by the BEM model are usually non-symmetric and dense, which is opposed to the FEM (the corresponding matrices generated by the FEM model are usually symmetric and sparse). This will significantly increase

the processing time and the storage requirements. Besides, at certain wave number values, the classical BEM solutions for the exterior acoustic problems are always nonunique. In order to deal with this difficulty, the classical BEM should be properly modified and the additional numerical treatments are needed. What is more, the BEM is restricted in the ability to handle the exterior acoustic problem in nonisotropic and nonhomogeneous media. In recent years, a novel singular boundary method (SBM) was proposed to handle the acoustic problems [Chen *et al.* (2014); Fu *et al.* (2014, 2015); Li *et al.* (2016); Chen and Wang (2016)]. In SBM, the concept of source factor is introduced to regularize the singularities of the fundamental solutions. The SBM successfully overcomes some drawbacks of the original BEM. Nevertheless, the mathematical theoretical analysis of the SBM seems to be not sufficiently complete and the relevant work is still on its way.

As an effective alternative to the classical BEM for exterior acoustic problems, the FEM is derived from the variational principle and has very firm mathematics foundations. In theory, the classical FEM has no limit in the wave number values and could solve the exterior acoustic problems with arbitrary large wave number values as long as the used meshes are sufficiently fine. In addition, the FEM can perform the coupling with complicated structures naturally and also can handle the problems in the nonisotropic and nonhomogeneous media. For BEM, these may be impossible or relatively difficult to implement. Nevertheless, the FEM for exterior acoustic problems is also not free of limit. Firstly, as a typical domain-based numerical technique, the conventional FEM cannot be directly used to handle the exterior acoustic problems because the involved problem domain is unbounded. In order to overcome this, the special techniques, which can enable the FEM to handle the problems in unbounded domains, are always required in general. These numerical techniques include the Dirichlet-to-Neumann (DtN) map [Keller and Givoli (1989); Giljohann and Bittner (1998)], the perfect matched layer [Berenger (1994)], the absorbing boundary conditions [Kim *et al.* (1996); Harari and Djellouli (2004)] and so on. Moreover, the FEM solutions for the general acoustic problems always suffer from the numerical error issue [Ihlenburg and Babuška (1995a); Deraemaeker *et al.* (1999)]. Due to the numerical error, the FEM solutions for the exterior acoustic problems are only relatively reliable for small wave number range; with the increase of the wave number values, the accuracy of the FEM solutions will degenerate rapidly. In practice, the above-mentioned numerical errors can be decomposed into two parts: the first part is the interpolation error. This kind of error is local and can be reduced by refining the used meshes. Actually, once the sufficient elements (at least six elements) are employed to discretize a wavelength, the interpolation error can be well-controlled. This is the well-known "rules of thumb". As opposed to the interpolation error, the pollution error is global and cannot be removed completely by using the refined meshes. Whether the "rules of thumb" are satisfied or not, the pollution effects exist all the same. More importantly, the pollution errors always remain in a relatively low level and can be neglected in the small wave number

range. With the increasing values of the wave number, the pollution errors will expand quickly and dominate the total error. This is indeed an intractable block in the application of the classical FEM to exterior acoustic problems.

With the aim to improve the quality of the FEM solutions for acoustic problems, many researches have been dedicated to this issue and a profusion of extended FEMs, stabilized FEMs and meshless techniques have been developed to cope with this issue. These techniques include the Galerkin/least-squares FEM (GLS-FEM) [Harari and Hughes (1992)], the generalized finite element method (GFEM) [Babuška *et al.* (1995)], the radial point interpolation method (RPIM) [Wenterodt and von Estorff (2009)], the element-free Galerkin method (EFGM) [Belytschko *et al.* (1994); Bouillard and Suleaub (1998)] and so on. Although all of these novel techniques could reduce the pollution errors considerably, the pollution effects for general acoustic problems still cannot be eradicated completely.

Recently, a series of smoothed finite element methods (SFEMs) were employed to solve the acoustic problems [He *et al.* (2009, 2012, 2014, 2015); Wang *et al.* (2015a, 2015b, 2016); Chai *et al.* (2016a, 2016b, 2016c)]. The SFEMs [Liu *et al.* (2007a, 2007b); Dai and Liu (2007); Nguyen-Xuan *et al.* (2008a); Bordas and Natarajan (2010); Bordas *et al.* (2011); Cui *et al.* (2015); Jiang *et al.* (2015); Zeng and Liu (2016); Zeng *et al.* (2016); Wan *et al.* (2016)], which is exactly the particular form of the smoothed interpolation methods (S-PIMs) [Liu and Zhang (2013); Zhang *et al.* (2015, 2016); Xu *et al.* (2016); Feng *et al.* (2016b); Wu *et al.* (2016)], are formulated by using the novel weakened weakform (or $\mathrm{W}^2$) based on the G space theory [Liu (2009); Chen *et al.* (2016)] and the gradient smoothing technique (GST) from the meshless methods [Nguyen *et al.* (2008); Liu (2016)]. Compared to the conventional FEM formulated from the standard Galerkin weakform, the SFEM could inject the softening effects into the standard FEM due to the $\mathrm{W}^2$ form and the GST. As a consequence, the system stiffness from SFEM behaves softer than that from the standard FEM and is closer to the exact stiffness of the continuous system. In the SFEMs, the related numerical integration is performed over the smoothing domains rather than the original elements. Actually, the SFEMs can be classified into several different forms according to the different types of the smoothing domains, such as the cell-based SFEM (CS-FEM) [Liu *et al.* (2013)], edge-based SFEM (ES-FEM) [Nguyen-Xuan *et al.* (2013); Cui and Chang (2015); Yang *et al.* (2016)], node-based SFEM (NS-FEM) [Nguyen-Thoi *et al.* (2010); Nguyen-Xuan *et al.* (2010); Vu-Bac *et al.* (2011); Hu *et al.* (2016); Liu *et al.* (2017)] and hybrid SFEM (HS-FEM or $\alpha$FEM) [Nguyen-Thanh *et al.* (2011); Chai *et al.* (2017); Li *et al.* (2017b)]. It is worth noting that different SFEMs usually possess different properties. For example, the CS-FEM with bilinear quadrilateral elements (or SFEM-Q4) is originally proposed by Liu *et al.* [2007a, 2007b] for solid mechanics. In this kind of SFEM, the original quadrilateral element is divided into $n_{\mathrm{s}} \in [1, +\infty]$ sub-smoothing domains. It is found that the SFEM-Q4 is less sensitive to the mesh distortion than the original FEM-Q4 because the traditional coordinate transformation program and the

mapping operations have been circumvented successfully. In addition, the SFEM-Q4 also possesses the important monotonic property and both the upper bound and lower bound of the solution can be obtained by adjusting the number of smoothing domains. The NS-FEM can usually provide the upper bound solutions for the solid mechanics and is immune from the volumetric locking issue for the nearly incompressible materials. However, the NS-FEM cannot be directly used to handle the dynamic and nonlinear problems due to its "overly-soft" properties. The ES-FEM can always provide models with very close-to-exact stiffness, therefore the ES-FEM often possesses the superconvergence property for general solid mechanics. In a word, all of these mentioned SFEMs have their own associated advantages and disadvantages. A very nice overview about the SFEMs can be seen in the monograph [Zeng and Liu (2016)]. The S-FEMs were initially employed to handle linear elastic solid mechanics problems [Liu *et al.* (2007a); Bordas *et al.* (2010); Cui *et al.* (2016); Feng *et al.* (2016a)]. Owing to the good and attractive properties, the S-FEMs have been applied to many other fields, such as fluid–structure interaction problems [Nguyen-Thoi *et al.* (2013)], acoustics [Li *et al.* (2014); Gong *et al.* (2016a); Hu *et al.* (2017); Wu *et al.* (2017); Li *et al.* (2017a)], plates and shells [Nguyen-Xuan *et al.* (2008b); Nguyen-Thanh *et al.* (2008); Li *et al.* (2016)], fracture mechanics problems [Chen *et al.* (2012); Vu-Bac *et al.* (2013); Nguyen-Thoi *et al.* (2014, 2017)], and heat transfer problems [Xue *et al.* (2013)].

The objective of the present work is to employ a smoothed finite element method with four-node quadrilateral elements (SFEM-Q4) [Dai and Liu (2007); Nguyen-Xuan *et al.* (2008a); Liu *et al.* (2013)] to resolve the underwater acoustic radiation problems. In this kind of SFEM, the traditional requirements of coordinate transformation procedure are not necessary to implement the numerical integration. For the purpose of truncating the unbounded domains and employing the domain-based numerical technique to tackle the acoustic radiation problems, the well-known DtN map is used to ensure that there are no spurious reflections from the far field. From the numerical tests, it is verified that the present SFEM-Q4 is quite effective to handle the acoustic radiation problems and the obtained numerical solutions are much more accurate than those from the standard FEM. The organization of the present work is as follows: the next section presents the governing equations for the exterior Helmholtz problems, the finite element formulations for the exterior acoustic problems are retrospected in Sec. 3; Sec. 4 includes the detailed formulation of SFEM-Q4 for acoustic problems; the numerical error estimate for the Helmholtz problems is given in Sec. 5; several typical numerical examples are analyzed and discussed in Sec. 6 and the final conclusions are summarized in Sec. 7.

## 2. The Governing Equations for the Exterior Helmholtz Problems

Supposing that the medium in the acoustic field is quiescent, compressible and uniform, and the acoustic wave is linear and harmonic. Then the acoustic pressure

$P$ can be governed by the following partial differential equation:

$$\nabla^2 P - \frac{1}{c^2}\frac{\partial^2 P}{\partial t^2} = 0, \tag{1}$$

in which $\nabla^2$ represents the Laplace operator, $c$ and $t$ stand for the speed of the acoustic wave and time, respectively.

Note that the acoustic wave is assumed to be harmonic, then the acoustic pressure $P(\mathbf{x})$ can be expressed by

$$P(\mathbf{x}) = p(\mathbf{x})\exp(j\omega t), \tag{2}$$

in which $p(\mathbf{x})$ represents the spatial distribution of the acoustic pressure amplitude, $j$ is the imaginary unit and $\omega$ denotes the angular frequency.

Then the well-known reduced acoustic wave equation (or the Helmholtz equation) can be obtained by

$$\nabla^2 p + k^2 p = 0, \tag{3}$$

in which $k$ is the wave number which is associated with $\omega$ and $c$ by $k = \omega/c$.

The above Helmholtz equation can be solved directly if a set of proper boundary conditions are complemented. Generally, the following three kinds of boundary conditions are usually considered, namely, the Dirichlet boundary condition ($\Gamma_D$), Neumann boundary condition ($\Gamma_N$) and Robin boundary condition ($\Gamma_R$). These boundary conditions can be expressed by

$$p = p_D \quad \text{on } \Gamma_D, \tag{4}$$

$$\frac{\partial p}{\partial n} = -j\rho\omega v_n \quad \text{on } \Gamma_N, \tag{5}$$

$$\frac{\partial p}{\partial n} = -j\rho\omega A_n p \quad \text{on } \Gamma_R, \tag{6}$$

in which $n$ is the outward unit normal vector to the corresponding boundary, $\rho$ denotes the density of the acoustic fluid, $v_n$ is the normal velocity on $\Gamma_N$ and $A_n$ stands for the admittance coefficient on $\Gamma_R$.

From Eqs. (4)–(6), we can find that the acoustic pressure $p$ is prescribed to be a fixed value $p_D$ on the Dirichlet boundary condition, the normal velocity $v$ condition is equal to a given value $v_n$ on the Neumann boundary and it is associated with the acoustic pressure $p$ by a fixed coefficient on the Robin boundary condition. For the exterior acoustic cases in which the involved problem domains are always unbounded, the corresponding governing equations are given by

$$\nabla^2 p + k^2 p + f = 0 \quad \text{in } R, \tag{7}$$

$$p = g \quad \text{on } \Gamma_D, \tag{8}$$

$$\frac{\partial p}{\partial n} = q \quad \text{on } \Gamma_N, \tag{9}$$

$$\lim_{r\to\infty} r^{\frac{(d-1)}{2}}\left(\frac{\partial p}{\partial r} - jkp\right) = 0 \tag{10}$$

in which $f$ contains the acoustic source term, $R$ stands for the involved problems domain which is unbounded, $g$ and $q$ are the prescribed functions which are associated with the Dirichlet data and Neumann data on the Dirichlet boundary and the Neumann boundary, respectively. $r$ denotes the distance from the origin and $d$ is the spatial dimension.

For the acoustic problems in the unbounded domains, the well-known Sommerfeld radiation condition should be satisfied so that only positive energy flux is allowed at infinity and there are no spurious reflecting waves from the far field, then the uniqueness of the solution for the above-mentioned boundary-value problem can be ensured. In addition, it is worth noting that the problem defined by Eqs. (7)–(10) cannot be solved directly by the conventional domain-based numerical techniques (such as the classical FEM) because the unbounded domain is involved. In order to enable the classical FEM to handle the exterior acoustic problem, the truncation boundary treatment is usually introduced to truncate unbounded domain and a bounded computational domain can be obtained. Then the exterior acoustic problem can be solved by the classical FEM. The related formulations will be given in the next section in detail.

## 3. Finite Element Formulation for the Exterior Acoustic Problems

As shown in Fig. 1, an object with arbitrary shapes is embedded in the unbounded domain $R$ and the surrounding acoustic fluid is quiescent and homogeneous. The surface of the object, which is denoted by $\Gamma$, is assumed to be piecewise smooth and it is delimited by $\Gamma = \Gamma_D \cup \Gamma_N$ and $\Gamma_D \cap \Gamma_N = \varnothing$, in which $\Gamma_D$ and $\Gamma_N$ are the relevant boundary conditions defined in the previous section. In order to obtain the required bounded computational domain, a circular artificial boundary $B$ (see Fig. 2) is introduced and the original unbounded domain is decomposed into two parts: the inside domain, which is internally bounded by the surface of the object and externally bounded by the artificial boundary $B$, is denoted by $\Omega_I$; the

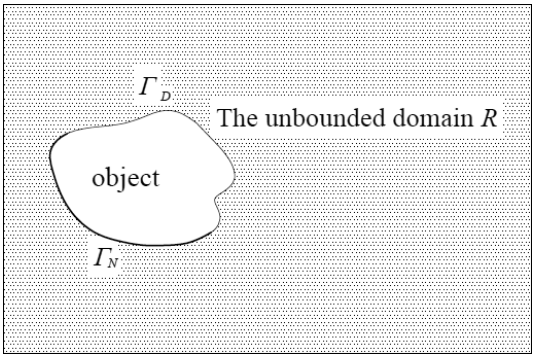


Fig. 1. The schematic illustration of exterior acoustic problems.

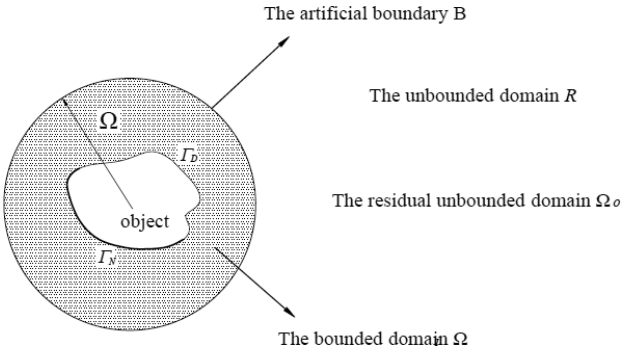


Fig. 2. The bounded computational domain is obtained by introducing an artificial boundary B.

outside domain $R - \Omega_I$, which is a residual unbounded domain, is denoted by $\Omega_O$. For the problem in the internal domain where all the source terms and geometric irregularities are contained within it, it can be solved by the finite element scheme easily and the related governing equations are given by

$$\begin{aligned} \nabla^2 p + k^2 p + f &= 0 \quad \text{in } R, \\ p &= g \quad \text{on } \Gamma_D, \\ \frac{\partial p}{\partial n} &= q \quad \text{on } \Gamma_N, \\ \frac{\partial p}{\partial n} &= -Mp \quad \text{on } B, \end{aligned} \tag{11}$$

in which $M$ is the so-called Dirichlet-to-Neumann (DtN) operator, it gives the relationship between the function value (the Dirichlet datum) and its normal derivative value (the Neumann datum) on the artificial boundary $B$. This DtN map is the exact impedance on $B$ and it will be discussed in the following context in detail.

According to Stewart and Hughes [1996], the standard Galerkin weak form for the above boundary-value problem is easy to formulate and it is defined by: Find $p \in S$ such that $\forall\, w \in V$($S$ denotes the trial solutions space and $V$ denotes the weighting functions space).

$$a(w,p) + b(w,p) = (w,f)_\Omega + (w,q)_\Gamma, \tag{12}$$

in which

$$a(w,p) = \int_\Omega (\nabla w \nabla p - k^2 wp) d\Omega, \tag{13}$$

$$b(w,p) = -\int_B w \frac{\partial p}{\partial n} dB \quad \text{on } B, \tag{14}$$

$$(w,f)_\Omega = \int_\Omega w f d\Omega, \tag{15}$$

$$(w,q)_\Gamma = \int_{\Gamma_N} w q d\Gamma. \tag{16}$$

At this stage, the crucial step for solving Eq. (12) is to compute the integral term $\int_B w\partial p/\partial n dB$. Once the related integration is carried out, the problem defined in the inside domain $\Omega_I$ can be solved easily.

The process of calculating the above-mentioned integration can be done by obtaining the exact solutions to the problem defined in the outside domain $\Omega_O$. After having solved this problem, the relationship between the acoustic pressure $p$ and its outward normal derivative $\partial p/\partial n$ on the artificial boundary $B$ can be obtained by

$$\frac{\partial p}{\partial n} = -Mp. \tag{17}$$

The above equation is the well-known DtN map. It gives the relationship between the Dirichlet datum ($p$) and the Neumann datum ($\partial p/\partial n$) on $B$. The sign $M$ is the DtN operator.

In the next step, we will begin to derive the explicit expression of the DtN operator $M$. In order to relatively easily solve the problem defined in the outside domain $\Omega_O$ by the analytical approach, the geometrical shape of the artificial boundary $B$ is usually constructed as easily as possible. A circle for two-dimensional case and a sphere for three-dimensional case are often used. For the two-dimensional problem domain considered in this paper, the corresponding analytical solution is easy to formulate and can be given by [Keller and Givoli (1989)]

$$p(r,\theta) = \frac{1}{\pi}\sum_{n=0}^{\infty}{}' \int_0^{2\pi} \frac{H_n^{(1)}(kr)}{H_n^{(1)}(kR)} \cos n(\theta-\theta')p(R,\theta')d\theta', \tag{18}$$

in which the sign ($'$) after the sum means that the corresponding value is halved for the first term, $H_n^{(1)}$ is the Hankel function of the first kind with $n$ order, $R$ is the radius of the circular artificial boundary $B$ and $p(R,\theta')$ is the prescribed Dirichlet data on $B$.

By performing the differentiation operation on Eq. (18) with respect to the argument $r$, we have

$$\left.\frac{\partial p(r,\theta)}{\partial n}\right|_{r=R} = -\sum_{n=0}^{\infty}{}' \int_0^{2\pi} m_n(\theta-\theta')p(R,\theta')d\theta'. \tag{19}$$

The normal derivative of the acoustic pressure $p$ on $B$ can be obtained from the above equation and the corresponding coefficient $m_n(\theta-\theta')$ is given by

$$m_n(\theta-\theta') = -\frac{k}{\pi}\frac{H_n^{(1)'}(kR)}{H_n^{(1)}(kR)}(\cos n\theta\cos n\theta' + \sin n\theta \sin n\theta'). \tag{20}$$

By substituting Eqs. (18) and (19) into Eq. (17), the DtN operator $M$ can be obtained easily and then Eq. (12) can be solved ultimately.

The finite element approximation of the acoustic pressure can be expressed by

$$p = \sum N_i p_i = \mathbf{N}\mathbf{p} \tag{21}$$

in which $p_i$ is the unknown nodal value associated with the node $i$ and $N_i$ corresponds to the FEM shape functions at node $i$.

Using the above approximated form of the acoustic pressure $p$ and the Green's formula, the finite element formulation for the exterior acoustic problems results in the following linear discretized equation:

$$[\mathbf{K} - k^2\mathbf{M} + \mathbf{K}^b_{AB}][\mathbf{P}] = [\mathbf{F}] \tag{22}$$

in which $\mathbf{P}$ is the vector of the unknown nodal acoustic pressure, $\mathbf{F}$ is nodal force vector, $\mathbf{K}$ and $\mathbf{M}$ are the so-called acoustical stiffness matrix and the acoustical mass matrix, respectively.

$$[\mathbf{P}]^T = [p_1,\ p_2, \ldots, p_n], \tag{23}$$

$$\mathbf{F} = -j\rho\omega \int_{\Gamma_N} \mathbf{N}^T v_n d\Gamma, \tag{24}$$

$$\mathbf{K} = \int_\Omega (\nabla\mathbf{N})^T \nabla\mathbf{N} d\Omega, \tag{25}$$

$$\mathbf{M} = \int_\Omega \mathbf{N}^T\mathbf{N} d\Omega. \tag{26}$$

In Eq. (22), the matrix $\mathbf{K}^b_{AB}$ corresponds to the DtN map and is given by

$$\begin{aligned}\mathbf{K}^b_{IJ} &= \int_B \mathbf{N}_I M \mathbf{N}_J dB \\ &= -\sum_{j=0}^{\infty} \frac{k}{\pi} \frac{H_n^{(1)'}(kR)}{H_n^{(1)}(kR)} \left(\int_B \mathbf{N}_I(\mathbf{x}) F_j(\mathbf{x}) dB\right) \left(\int_B \mathbf{N}_J(\mathbf{x}) F_j(\mathbf{x}') dB\right)\end{aligned} \tag{27}$$

in which $\mathbf{N}_I$ and $\mathbf{N}_J$ are the shape functions corresponds to node $I$ and node $J$, the simple trigonometric functions $F_j(\mathbf{x})$ and $F_j(\mathbf{x}')$ are given by

$$F_j(\mathbf{x}) = [\cos n\theta\ \ \sin n\theta], \tag{28}$$

$$F_j(\mathbf{x}') = \begin{bmatrix}\cos n\theta' \\ \sin n\theta'\end{bmatrix}. \tag{29}$$

From Eq. (22), it is clearly found that an additional term $\mathbf{K}^b_{AB}$ is added to the original finite element formulation for the exterior Helmholtz equation due to the DtN map. However, it is relatively easy to obtain the matrix $\mathbf{K}^b_{AB}$ because only the boundary integrals on the artificial boundary have to be computed. Therefore, the process of incorporating the DtN map into the original finite element formulation for exterior Helmholtz problems can be implemented without increasing efforts. What is more, from Eq. (27), we can find that the process of calculating the matrix $\mathbf{K}^b_{AB}$ does not depend on the wave number $k$. This obviously distinguishes from

the classical BEM for exterior problems (where the related surface integration has a dependence on the wave number $k$ and it has to be re-computed for each wave number value), so the additional computational demands for evaluating the boundary integrals in Eq. (27) can be neglected. Nevertheless, since the DtN map used in this work is non-local, then the obtained matrix $\mathbf{K}_{AB}^{b}$ is not sparse and banded in general. Therefore, the sparseness of the original acoustic stiffness $\mathbf{K}$ may be spoiled and the corresponding bandwidth may be increased, and then additional computational cost and storage requirements are needed. However, it is found that the sparseness of the original acoustic stiffness $\mathbf{K}$ can be maintained by carefully numbering the nodes on the artificial boundary $\mathbf{B}$ [Giljohann and Bittner (1998)]. Numerical tests demonstrate that the DtN map is quite effective to handle the exterior Helmholtz problems.

In addition, it is worth noting that the full DtN map involves infinite terms and it cannot be implemented in practical numerical computation. Therefore, it is usually truncated at some limit (at a maximum limit $n_{\max}$). Besides, the radius of the artificial boundary $R$ also plays an important role in performing the DtN map. In general, the accuracy of the numerical solutions will improve with the increase of the radius $R$ and the maximum $n_{\max}$ used in the DtN map. However, large values of $R$ will always lead to fairly expensive computational cost. As opposed to this, if the value of $R$ is too small, the largish round-off errors will arise and the accuracy of the numerical solutions will be compromised substantially. On the other hand, the truncation error is always inevitable if the truncated DtN map is used. The large number of terms of the DtN map is helpful to reduce this truncation error, but the excessive terms of the DtN map are not recommended because it always increases the consuming time rather than improving the quality of the numerical solution. In practical computation, we have to balance the accuracy of the numerical solutions and the computational cost when choosing the two above-mentioned parameters. According to Keller and Givoli [1989], there exists an optimal $n$ ($n_{\text{opt}}$) for the average mesh size $h$ and the fixed $R$. This value $n_{\text{opt}}$ occurs when the finite element discretization error equals the truncation error of the DtN map. According to Keller and Givoli [1989], the optimal $n$ ($n_{\text{opt}}$) and the value of $R$ satisfy the following formula:

$$n_{\text{opt}} = -(l+1)\frac{\log_{10}(h)}{\log_{10}(R)}, \tag{30}$$

in which $l$ stands for the degree of the used FEM shape functions which is the polynomial form.

Though the above formula is only a crude estimate, large numbers of numerical tests show that the chosen values of the two parameters using Eq. (30) are quite effective and reasonable. In this work, unless otherwise specified, $n_{\max} = 40$ and $R = 1.2$ are directly used to perform the practical computation for all the numerical tests. Numerical results show that the above values of the two parameters are sufficient to ensure the accuracy of the numerical solutions.

## 4. Formulation of SFEM-Q4 for Acoustic Problems

In this section, the formulation of the SFEM-Q4 and the process of performing the GST will be presented in detail. As shown in Fig. 3, the background elements in the involved problem domain $\Omega(\Omega = \cup_{i=1}^{N_e}\Omega_i^e$ and $\Omega_i^e \cap \Omega_j^e = \varnothing$, $i \neq j$, $N_e$ is the total number of the quadrilateral elements) used in the SFEM-Q4 are exactly the same as those used in the standard FEM. In order to perform the gradient smoothing operations, $n_e^s \in [1, +\infty]$ sub-quadrilateral elements, which are not only nonoverlapping but also no-gap, are obtained by further dividing (the further divide operation is performed by linking the mid-points of the opposite segments) each element $\Omega_i^e$, such that $\Omega_i^e = \cup_{m=1}^{n_e^s}\Omega_{i,m}^s$. These obtained sub-quadrilateral elements are the so-called smoothing domains (SDs). As a consequence, the involved problem domain is divided into $N_s = N_e \times n_e^s$ SDs and the GST will be performed over these SDs.

Therefore, for acoustic problems, the smoothed system stiffness matrix for the smoothing domain $\Omega_{i,m}^s$ can be obtained by

$$\overline{\mathbf{K}}_{i,m}^s = \int_{\Omega_{i,m}^s} (\overline{\nabla \mathbf{N}})^T \overline{\nabla \mathbf{N}} d\Omega. \tag{31}$$

The relationship between the acoustic pressure gradient and the acoustic particle velocity can be expressed by

$$\nabla p + j\rho\omega v = 0. \tag{32}$$

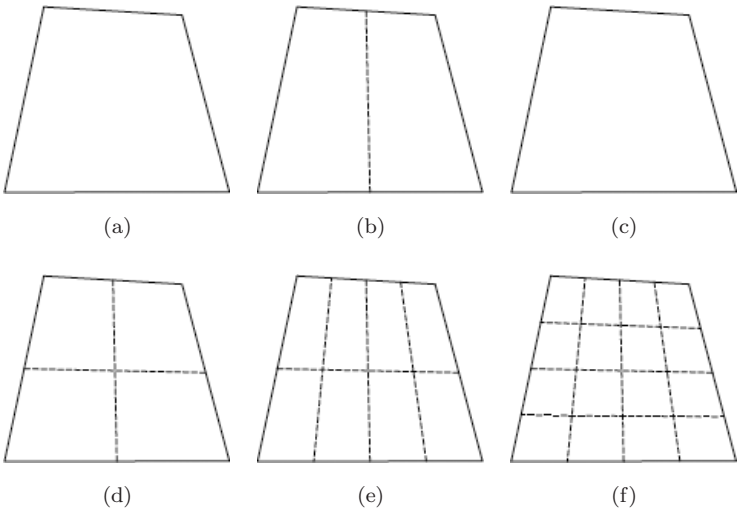


Fig. 3. The original quadrilateral element $\Omega_i^e$ is divided into $n_e^s \in [1, +\infty]$ smoothing domains by linking the mid-points of the opposite segments: (a) 1SD; (b) 2SDs; (c) 3SDs; (d) 4SDs; (e) 8SDs; (f) 16 SDs.

In the present formulation, the gradient smoothing operations are performed by smoothing the acoustic particle velocity in the acoustic field and then the smoothed particle velocity $\bar{\mathbf{v}}(\mathbf{x})$ in each smoothing domain $\Omega^s$ can be obtained by

$$\bar{\mathbf{v}}(\mathbf{x}) = \int_{\Omega^s} \mathbf{v}(\mathbf{x})\Phi(\mathbf{x})d\Omega, \tag{33}$$

in which $\Phi(\mathbf{x})$ denotes a particular smoothing function which should satisfy the following property

$$\int_{\Omega^s} \Phi(\mathbf{x})d\Omega = 1. \tag{34}$$

For simplification, the smoothing function $\Phi(\mathbf{x})$ is usually chosen by

$$\int_{\Omega^s} \Phi(\mathbf{x})d\Omega = 1, \tag{35}$$

in which $A^s = \int_{\Omega^s} d\Omega$ is the area of the smoothing domain $\Omega^s$.

Substituting Eq. (32) into Eq. (33) and using the divergence theorem, we have

$$\bar{\mathbf{v}}(\mathbf{x}) = -\frac{1}{j\rho\omega A^s}\int_{\Omega^s} \nabla p d\Omega = -\frac{1}{j\rho\omega A^s}\int_{\Gamma^s} p \cdot n d\Gamma, \tag{36}$$

in which $\Gamma^s$ is the boundary of the smoothing domain $\Omega^s$ and $n$ is the outward normal vector.

Using the approximate form of the acoustic pressure defined in Eq. (21), we have

$$\bar{\mathbf{v}}(\mathbf{x}) = -\frac{1}{j\rho\omega}\sum_{i\in M_k} \bar{\mathbf{B}}_i(\mathbf{x})p_i, \tag{37}$$

in which $M_k$ is the number of involved nodes in the smoothing domain, $\bar{\mathbf{B}}_i(\mathbf{x})$ denotes the smoothed gradient matrix and can be computed using the Gauss integration scheme and is given by

$$\bar{\mathbf{B}}_i(\mathbf{x}) = \frac{1}{A^s}\int_{\Gamma^s} \mathbf{N}_I(x)\begin{bmatrix} n_x \\ n_y \end{bmatrix} d\Gamma = \frac{1}{A^s}\sum_{q=1}^{N_s}\left(\sum_{r=1}^{N_g} w_r \mathbf{N}_I(x)\begin{bmatrix} n_x \\ n_y \end{bmatrix}\right), \tag{38}$$

in which $N_s$ is the segment number of the boundary $\Gamma^s$, $N_g$ is the number of the Gauss points (only one Gauss point is needed since the used shape function is linear) distributed in each segment and $w_r$ is the corresponding weighting coefficients, $n_x$ and $n_y$ are the components of the outward normal vector along the boundary $\Gamma^s$.

From Eqs. (36) and (38), it is found that the traditional mapping and coordinate transformation step is not needed when performing the GST, and the required area integration over the smoothing domain becomes the line integration along the boundary of the smoothing domain. Therefore, only the shape function values (not the derivatives of the shape function) at the quadrature points are required. This allows us to construct the shape functions in more flexible way. For the quadrilateral elements (Q4) used in this paper, the conventional bilinear shape functions are employed and the shape function values at the Gauss points are evaluated by the

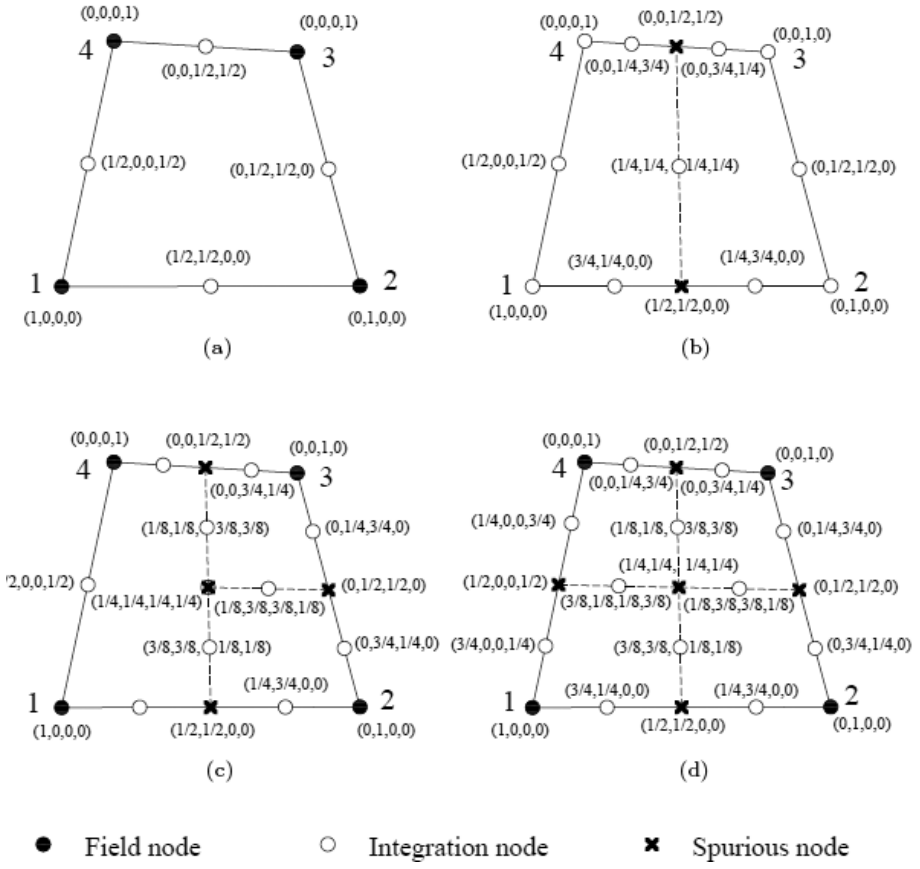


Fig. 4. The shape function values at the quadrature points distributed along the boundary of the smoothing domains: (a) 1SD; (b) 2SDs; (c) 3SDs; (d) 4SDs.

two related endpoints of the segment containing the Gauss point (see Fig. 4), for the convenience of notation, the format ($N_1$, $N_2$, $N_3$, $N_4$) is used in the figure. Once all the shape function values at the Gauss points are acquired, the smoothed gradient matrix in Eq. (38) can be obtained easily.

Then the smoothed acoustical stiffness matrix for the smoothing domain can be calculated by

$$\bar{\mathbf{K}}^s = \int_{\Omega^s} \bar{\mathbf{B}}^T \bar{\mathbf{B}} d\Omega = \bar{\mathbf{B}}^T \bar{\mathbf{B}} A^s. \tag{39}$$

Finally, the global smoothed acoustical stiffness matrix can be assembled by

$$\bar{\mathbf{K}}^s = \sum_{s=1}^{N_s} \bar{\mathbf{K}}^s. \tag{40}$$

It should be noted that the SFEM-Q4 is exactly identical to the FEM using reduced integration if the number of smoothing domain in each quadrilateral element equals

$1(n_e^s = 1)$. In this case, the SFEM-Q4 is variationally consistent and it has been proven by Liu *et al.* [2007a]. What is more, the upper bound solution for solid mechanical problem can be obtained by this kind of SFEM-Q4 ($n_e^s = 1$). However, with the increase of the value of $n_e^s$, the solution from SFEM-Q4 will approach gradually the solution from the standard compatible FEM using full integration and the corresponding lower bound solution can be obtained. More importantly, the process of changing the solution from upper to lower bound is monotonic with the increasing $n_e^s$. Actually, there exists an optimal value of $n_e^s$. If this value of $n_e^s$ is used, the solutions from SFEM-Q4 are closes to the exact solutions. For the acoustic problems considered in this paper, the computational experience [Yao *et al.* (2010, 2016)] suggests that $n_e^s = 4$ always leads to stable numerical solutions and the obtained numerical results are always closer to the exact ones than the standard FEM. Therefore, $n_e^s = 4$ (see Fig. 4(d)) is used for all the numerical examples in this paper.



## 5. Numerical Error Estimate for the Helmholtz Problems

As is well known to all, the quality of the FEM solutions for the Helmholtz problems is usually affected by the numerical error which can be regarded as the difference between the numerical wave number $k'$ and the exact wave number $k^e$. For a fixed mesh pattern, the numerical error is closely associated with the wave number $k$: the larger the wave number $k$ is, the larger the numerical error will be. In general, the numerical error effects cannot be removed completely whether or not the used mesh is sufficiently fine. Actually, the Helmholtz equation with large wave numbers has been considered as a well-known unsolved problem of the classical finite element method [Zienkiewicz (2000)]. In practical engineering application, the FEM researchers usually follow the so-called "rule of thumb" to retain the accuracy of the FEM solutions for Helmholtz problems. In this criterion, a fixed number of elements should be used to resolve a wavelength. However, a plenty of numerical examples show that the FEM solutions of Helmholtz problems are only reliable for a relatively low wave number range if the above criterion is held. With the increase of the wave number, the numerical error will still expand dramatically and the obtained numerical solutions will be unreliable.

In order to estimate the numerical error of the finite element approximation for the Helmholtz problems, the numerical error indicator introduced by Ihlenburg *et al.* [1997] is defined by

$$E_p = |p^e - p'|_1^2 = \int_\Omega (\tilde{v}^e - \tilde{v}')^T (v^e - v') d\Omega, \tag{41}$$

in which the symbol "$\sim$" stands for the complex conjugate of the corresponding variable, $v$ represent the acoustic particle velocity, the symbol "$e$" and the prime denote the exact solution and the numerical solution for the Helmholtz equation, respectively.

Ihlenburg and Babuška [1995a, 1995b, 1997] have proved that the relative numerical error of the finite approximation for the Helmholtz problems are bounded by

$$\eta = \frac{|p^e - p'|_1}{|p^e|_1} = \sqrt{\frac{\int_\Omega (\tilde{v}^e - \tilde{v}')^T (v^e - v') d\Omega}{\int_\Omega (\tilde{v}^e \cdot v^e) d\Omega}} \leq C_1 \left(\frac{kh}{l}\right)^l + C_2 k \left(\frac{kh}{l}\right)^{2l}, \quad (42)$$

in which $l$ is the degree of the used polynomial shape function, $C_1$ and $C_2$ are the related constants which are independent of the wave number $k$ and the average mesh size $h$.

For the linear functions discussed here, the relative numerical error can be rewritten by

$$\eta \leq C_1 kh + C_2 k^3 h^2. \quad (43)$$

The above equation shows that the above-mentioned relative numerical error is made of two different parts. The first part in Eq. (43), which can be regarded as the interpolation error, is associated with the non-dimensional wave number $kh$. This kind of error is the local error and will be under control as long as $kh =$ constant is kept. This actually corresponds to the so-called "rule of thumb" in which a certain number of elements should be taken to discretize a wavelength. The second part in Eq. (43), which is named as the dispersion error (or pollution error) in some literatures, has an additional dependence on the wave number $k$ compared to the interpolation error. In contrast to the interpolation error, the dispersion error is the global error. From Eq. (43), it is clearly seen that only following the rule of thumb is not sufficient to control the dispersion error and it will grow linearly with the increase of the wave number $k$. Actually, using the rule of thumb can only lead to relatively reliable solutions in a small wave number range because the main source of the numerical error is the interpolation error and the dispersion error is small (can be neglected) in this case. However, with the increase of the wave number, the dispersion error will expand quickly and dominate the total numerical error. For the purpose of controlling the dispersion error, the related term $k^3h^2$ should be kept constant. This means that the well-refined meshes should be used for large wave number values. There have been many efforts to control the interpolation error and the dispersion error using the new numerical techniques in the past few decades. In this work, the performance of the proposed SFEM-Q4 with quadrilateral elements in controlling the interpolation error and the dispersion error for the Helmholtz problems will be examined and discussed in detail.

## 6. Numerical Results

### 6.1. *Circumferentially harmonic radiation from an infinite cylinder*

As shown in Fig. 5, the first considered problem is related to an infinite length oscillating cylinder with order $n$, namely the load distribution $\cos n\theta$ is considered here. This is a very common and simple acoustic radiation problem. The rigid cylinder

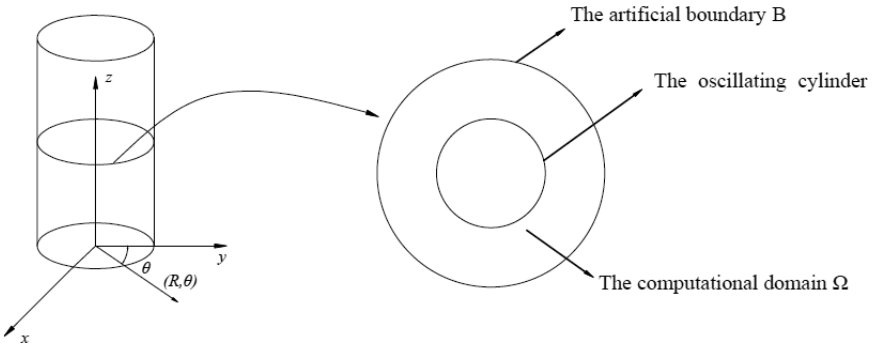


Fig. 5. The schematic description of circumferentially harmonic radiation from an infinite cylinder.

of radius $a = 0.5$ is embedded in the three-dimensional unbounded domain and the surrounding acoustic medium is water (density $\rho = 1000\,\mathrm{kg/m^3}$ and acoustic wave speed $c = 1500\,\mathrm{m/s}$). Note that one of the involved dimensions in this problem is much larger than the other two and all the variables along the $z$-axis are constants, hence this three-dimensional problem can be simplified into a typical two-dimensional problem. The circular artificial boundary with radius $R = 1.2$ is centered at (0, 0) and the obtained computational domain is divided into uniform quadrilateral elements and triangular elements (see Fig. 6). This typical acoustic radiation problem has been studied many times by Harari and Hughes [1992] before.

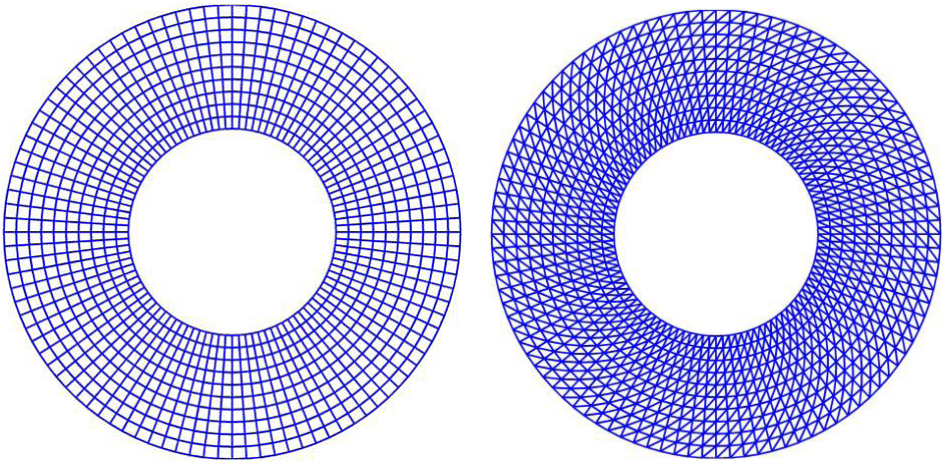

(a) (b)

Fig. 6. The mesh pattern of the involved computational domain: (a) quadrilateral elements; (b) triangular elements.

The exact solution to this problem is easy to formulate and can be expressed as

$$p(r,\theta) = \frac{H_n^1(kr)}{H_n^1(ka)}\cos(n\theta), \tag{44}$$

in which $H_n^1$ stands for the Hankel functions of the first kind of order $n$.

### 6.1.1. *Accuracy study*

Firstly, the validity and feasibility of the present SFEM-Q4 for acoustic radiation problems will be examined by solving the above-mentioned problem. For the convenience of discussion and comparison, three different non-dimensional wave numbers ($ka = 3$, $ka = 6$, $ka = 9$ and $ka = 12$) are employed in practical computation. For the forth circumferential mode $n = 3$, the imaginary part of the radiated pressure at a distance of $R = 1$ m from the center of the artificial boundary obtained from the FEM-Q4 and the present SFEM-Q4 are shown in Fig. 7. The corresponding

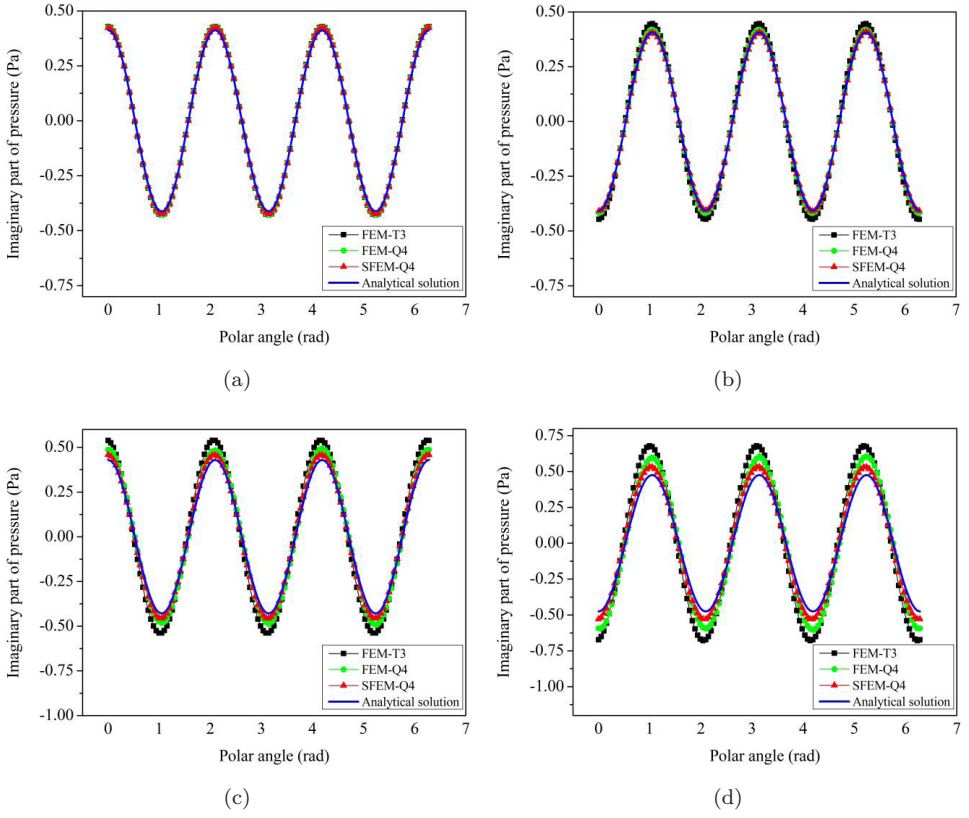


Fig. 7. The imaginary part of the radiated pressure at a distance of $R = 1$ m from the center of the artificial boundary obtained from different numerical techniques for circumferentially harmonic radiation: (a) $ka = 3$; (b) $ka = 6$; (c) $ka = 9$; (d) $ka = 12$.

numerical results from FEM with triangular elements (FEM-T3) and the exact solution are also plotted in the figures. From these figures, it is clearly seen that all the results from the numerical methods (FEM-T3, FEM-Q4 and SFEM-Q4) are in accordance with the exact solutions at the small wave numbers. As the wave number gets larger, the SFEM-Q4 results will stand out obviously and be superior to the results from the other two numerical methods with the identical node distributions. These findings indicate that the GST used in the SFEM-Q4 helps to properly soften the stiffness of the original "overly-stiff" discretized numerical model, and hence better results could be achieved.

### 6.1.2. *The effects of mesh distortion*

For the standard four-node isoparametric elements, it is known that the mapping operations are required to perform the coordinate transform process from the physical coordinate system to the natural coordinate system. In order to guarantee the correspondence property of the transform process, the concave elements are not permitted. Actually, the standard FEM-Q4 is sensitive to mesh distortion and the accuracy of the obtained numerical solutions will degrade if the severely distorted meshes are used. In this section, the effects of distorted meshes on the accuracy of the results from different methods will be investigated. The used irregular mesh is shown in Fig. 8. The irregular mesh is obtained from the regular mesh by introducing an irregularity factor $\beta$ in the following ways:

$$\begin{aligned} x' &= x + \Delta x \cdot r_c \cdot \beta, \\ y' &= y + \Delta y \cdot r_c \cdot \beta, \end{aligned} \tag{45}$$

in which $x'$ and $y'$ denote the coordinates of the nodes for the irregular mesh; $x$ and $y$ are the initial coordinates of nodes for the regular mesh; $\Delta x$ and $\Delta y$ represent the

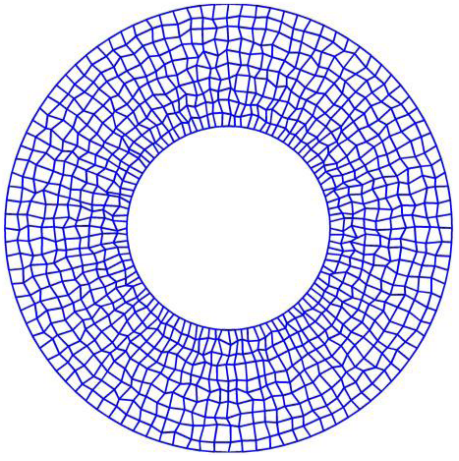

Fig. 8. The used irregular mesh for the involved problem domain.

average nodal space in the $x$ and $y$ directions, respectively; $r_c = [-1, 1]$ are a series of random numbers; $\beta$ is an irregularity factor and its value is generally between 0 and 0.5.

For the non-dimensional wave number $ka = 3\pi$, the imaginary part of the radiated acoustic pressure at a distance of $R = 1\,\mathrm{m}$ from the center of the artificial boundary is computed and shown in Fig. 9. For the convenience of comparison and discussion, the exact solution together with the numerical results from FEM-Q4 and SFEM-Q4 using different meshes is plotted in the figure. From the figure, it is seen that the quality of the numerical results will get worse if the distorted

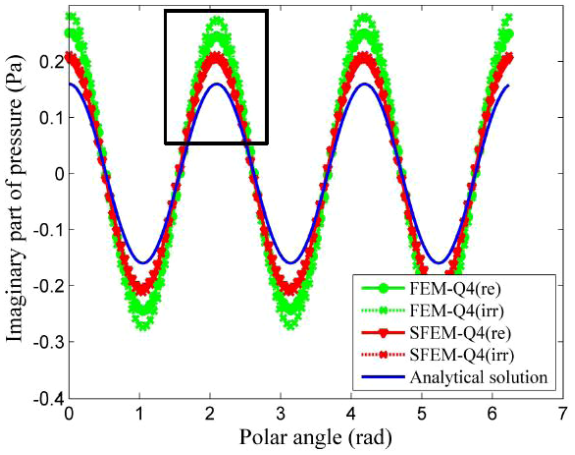


(a)

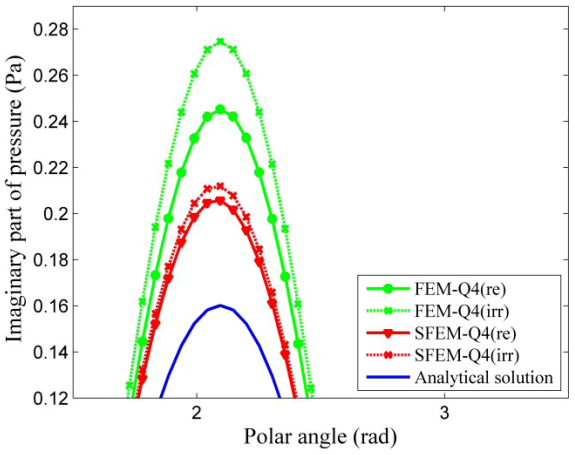


(b)

Fig. 9. The numerical results of the radiated acoustic pressure from different methods using different meshes: (a) Full scale distribution; (b) Zoomed-in distribution.

mesh is used for both FEM-Q4 and SFEM-Q4. In terms of FEM-Q4, the accuracy of the numerical results degrade very much when using the irregular mesh. However, the SFEM-Q4 results only change a little when the regular mesh is replaced by the irregular mesh. These fundamental findings indicate that the present SFEM-Q4 is less sensitive to the mesh distortion than the original FEM-Q4. The possible reason for this may be that only the corresponding line integration is needed to compute and the traditional coordinate transformation program has been circumvented successfully in the process of performing the gradient smoothing operations [Liu *et al.* (2007a, 2007b); Nguyen-Xuan *et al.* (2008a)].

### 6.1.3. *Convergence study*

We have known that the present SFEM-Q4 behaves better and can provide more accurate numerical results for acoustic radiation problems than the FEM-Q4 with the same mesh. The convergence properties of the SFEM-Q4 will be studied here. To perform the convergence study, several uniform and regular meshes with different average mesh sizes are employed. The relative numerical error $\eta$ obtained from the three different numerical methods (SFEM-Q4, FEM-Q4 and FEM-T3) versus the parameter $1/h$ ($h$ stands for the average mesh size) is depicted in Fig. 10. In order to take the effects of wave number into consideration, both small wave number value ($k = 4\pi$) and large wave number value ($k = 8\pi$) are considered. From the numerical results shown in the figure, the following findings can be easily obtained:

(1) For all the three used numerical techniques, the relative numerical error results at small wave number value ($k = 4\pi$) are obviously smaller than the counterparts at large wave number value ($k = 8\pi$). It is very easy to understand this because the relative numerical error will generally get larger with the increase of the wave number.

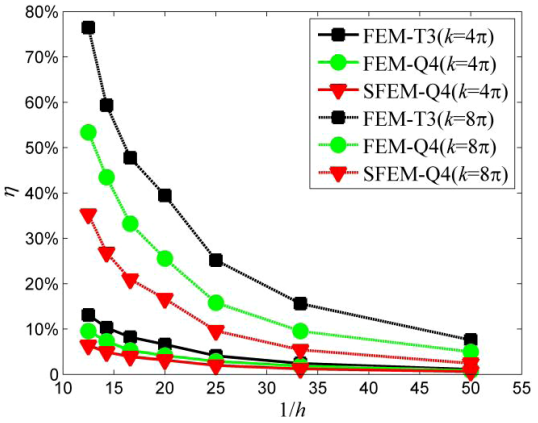


Fig. 10. The relative numerical error results from the three numerical techniques versus the parameter $1/h$ for different wave number values.

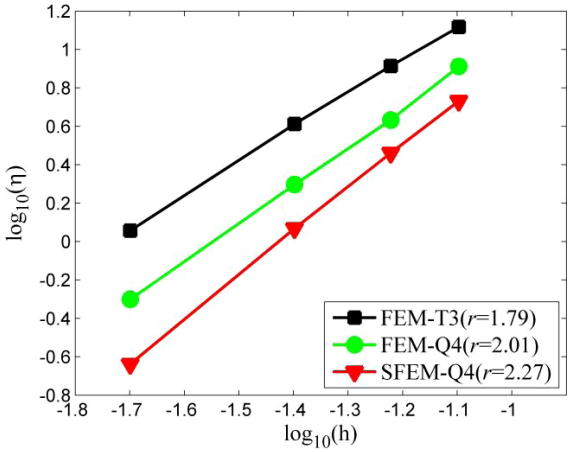


Fig. 11. The convergence rate results for SFEM-Q4, FEM-Q4 and FEM-T3.

(2) For the same mesh, the present SFEM-Q4 results are clearly better than the FEM-Q4 and FEM-T3 results. This indicates that the original "overly-stiff" numerical model is properly softened by the gradient smoothing operations and then more accurate numerical results can be obtained.
(3) For both the small wave number value ($k = 4\pi$) and the larger wave number value ($k = 8\pi$), the relative numerical error results from all the used numerical methods will tend to zero if the used mesh gets finer. However, the present SFEM-Q4 results converge evidently faster than the FEM-Q4 and FEM-T3 results. It is suggested that the SFEM-Q4 possesses faster convergence properties than the original FEM-Q4 and FEM-T3 for the acoustic radiation problems.

In order to study the convergence property of the SFEM-Q4 more clearly, for the fixed wave number $k = 4\pi$, the convergence rate results for three different numerical approaches are also calculated and discussed here (see Fig. 11). From Fig. 11, it is obvious that the present SFEM-Q4 ($r = 2.27$) converges faster than the FEM-Q4 ($r = 2.01$) and FEM-T3 ($r = 1.79$). These findings indicate that the present SFEM-Q4 possesses faster convergence rate property than the FEM-Q4 and FEM-T3 for acoustic radiation problems.

### 6.1.4. *Control of the numerical error*

The behavior of the present SFEM-Q4 in controlling the numerical error for acoustic radiation problems will be investigated in this section. From the formulation presented in Sec. 5, it is clear that both the wave number $k$ and the quality of the used meshes can affect the numerical error. In general, for a fixed mesh pattern, the larger the wave number $k$ is, the larger the numerical error will be. This is because both the interpolation error and the dispersion error (or pollution error) will expand with the increase of the wave number $k$. On the other hand, for a given

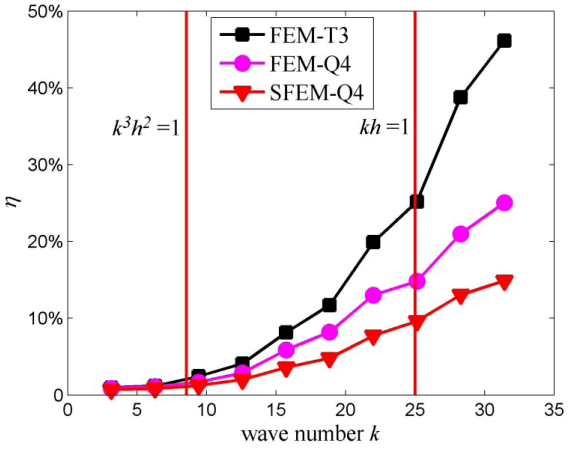


Fig. 12. The relative numerical error results from different numerical methods versus the wave number $k$.

wave number $k$, the numerical error results will also become smaller if the quality of the used mesh gets better. Therefore, with the aim to clearly study the performance of the numerical methods in controlling the numerical error, both the wave number $k$ and the quality of the used meshes should be taken into consideration.

Firstly, the behavior of the several mentioned numerical methods in controlling the numerical error will be examined by performing the related numerical computation on a range of wave number values for a fixed mesh pattern. Figure 12 shows the relative numerical error results from different numerical methods versus the wave number $k$. From Eq. (42), it is seen that the relative numerical error can be decomposed into two different parts, namely the interpolation error term (which is related to $kh$) and the dispersion error term (which is related to $k^3h^2$). In several published literatures, $kh$ and $k^3h^2$ are also named as the pre-asymptotic and asymptotic estimate, respectively. For the convenience of analysis and discussion, the case of $kh = 1$ and $k^3h^2 = 1$ is also plotted in the figure. From the figure, we can find that the relative numerical error results from all the different numerical methods are very small for low wave number range ($k^3h^2 < 1$). As the wave number $k$ increases, the corresponding relative numerical error results will expand quickly for all the methods. However, the behavior of the present SFEM-Q4 in controlling the numerical error is the best compared to the FEM-Q4 and FEM-T3, and this phenomenon will be even more outstanding for the relatively large wave number range ($kh > 1$). This indicates that a certain level of the numerical errors have been controlled by the present SFEM-Q4, and hence the SFEM-Q4 results are better than the FEM-Q4 and FEM-T3 results.

Furthermore, in order to study the numerical error in more detail, the relative numerical error results are calculated on a range mesh with different average sizes. Figure 13 plots the relative error results versus the parameter $1/h$ ($h$ stands for

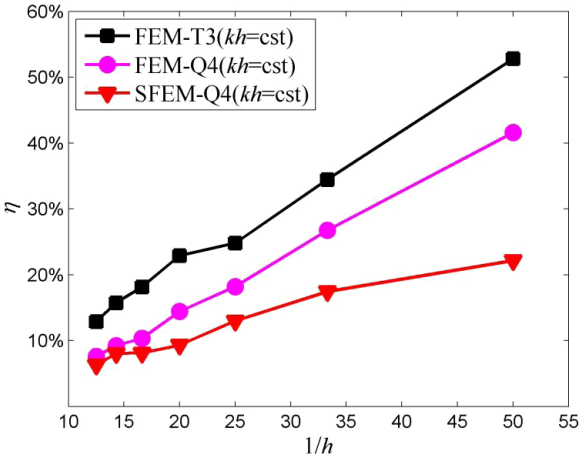


Fig. 13. The relative numerical error results versus the parameter $1/h$ in the case of keeping $kh$ = constant.

the average mesh size of the used mesh) for the three numerical methods in the case of keeping $kh$ = constant. From the plot, we can easily find that the relative numerical error is kept very small in the low wave number range and will expand very quickly with the increase of the parameter $1/h$ (namely the wave number $k$ because $kh$ = constant). The possible reason for this may be that both the interpolation error ($kh = 1$) and the dispersion error ($k^3h^2 = 1$) are very small and can be neglected for the small wave numbers. However, as the wave number $k$ increases, the dispersion error will grow linearly with $k$ even if the interpolation error can be controlled by keeping $kh$ = constant. This also exactly gives the reason why the so-called "rules of thumb" (namely $kh$ = constant is kept) are not sufficient to control the numerical error well for acoustic problems. Nevertheless, it can still be found that the present SFEM-Q4 behaves better and is less sensitive to the increasing wave number $k$ than the FEM-Q4 and FEM-T3. Figure 14 plots the relative numerical error versus the parameter $1/h$ for the three mentioned numerical methods in the case of keeping $k^3h^2$ = constant. The results in the figure reveal that the relative numerical error can be well controlled for all the three numerical methods if $k^3h^2$ = constant is kept. This is because both the interpolation error and the dispersion error can be controlled in the case of $k^3h^2$ = constant. However, the relative numerical error results from the SFEM-Q4 are still smaller than those from the FEM-Q4 and FEM-T3. From the above comparison and discussion, it is demonstrated that the behavior of the present SFEM-Q4 in controlling the relative numerical error is similar as the FEM-Q4 and FEM-T3. Although the numerical error in the acoustic radiation problems cannot be removed completely by the present SFEM-Q4, the quality of the FEM-Q4 results can be improved significantly by the present SFEM-Q4.

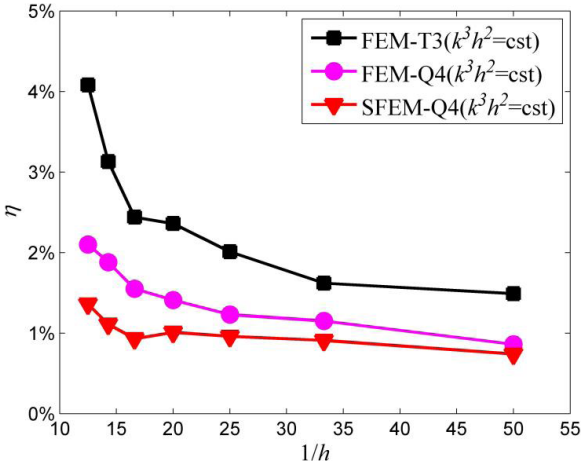


Fig. 14. The relative numerical error results versus the parameter $1/h$ in the case of keeping $k^3h^2 =$ constant.

### 6.1.5. *Computational efficiency study*

From the above analysis and discussion, we have known that the present SFEM-Q4 can provide better numerical results and is more effective to control the numerical error for acoustic radiation problems than the standard FEM-Q4 with the identical node distributions. However, in order to perform the GST, some pre-processing operations are needed and this will increase the consuming time. Therefore, whether or not the present SFEM-Q4 is more numerically effective for acoustic radiation than the FEM-Q4 still remains unclear. In this section, the computational efficiency of the three above-mentioned numerical techniques (SFEM-Q4, FEM-Q4 and FEM-T3) for acoustic radiation problems will be compared and discussed. To perform the computational efficiency study, several mesh patterns with different average sizes are used in the practical computation and all the programs are compiled in the same hardware environment. For the fixed non-dimensional wave number $ka = 9$, the CPU time (s) versus the total degree of freedoms for the three mentioned numerical methods is given in Fig. 15. From the figure, we can clearly find that the computational cost of the present SFEM-Q4 is more expensive than the FEM-Q4 and FEM-T3 if the identical node distributions are used. This is easy to understand because the extra pre-processing operations are required in the present SFEM-Q4, but it does not mean that the SFEM-Q4 is less numerically effective than the FEM-Q4 and FEM-T3. To investigate the computational efficiency of the present SFEM-Q4 more clearly, the CPU time (s) of the three different numerical techniques versus the numerical error indicator are shown in Fig. 16. From the figure, the computational efficiency of the SFEM-Q4 will clearly surpass the FEM-Q4 and FEM-T3 if the numerical error indicator is taken into consideration (the

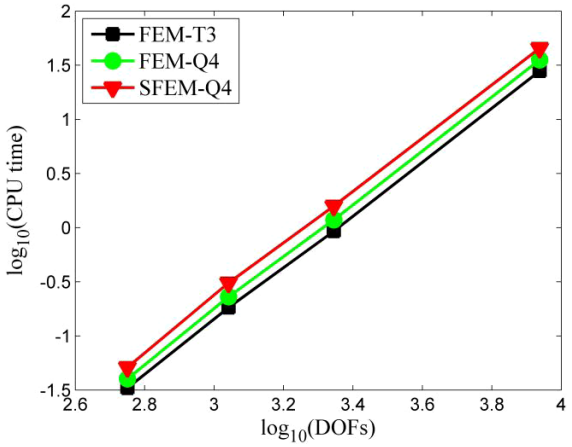


Fig. 15. The computational cost of the three different numerical techniques versus total degree of freedoms.

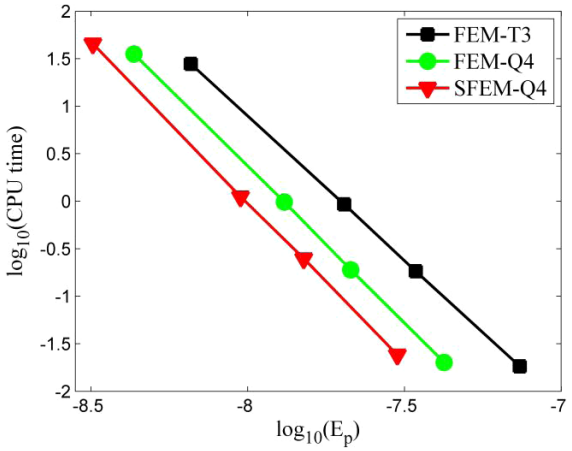


Fig. 16. The computational cost of the three different numerical techniques versus the numerical error indicator.

CPU time for the same numerical error). This means that the SFEM-Q4 possesses higher computational efficiency than the FEM-Q4 and FEM-T3, and fairly reliable numerical results for the acoustic radiation problems could be obtained by using the relatively coarse meshes.

### 6.2. *Radiation from a portion of the infinite cylinder*

The numerical example considered in the previous section is relatively simple. Now a more complicated problem will be considered to further validate the effectiveness of the present method. To this end, only partial arc ($-\alpha < \theta < \alpha$) of the cylinder

is prescribed to a constant inhomogeneous loading and this loading will vanish elsewhere. The analytical solution to this non-uniform radiation problems is easy to formulate and the exact radiated acoustic pressure can be given by

$$p(r,\theta) = \frac{2}{\pi}\sum_{n=0}^{\infty}{}' \frac{\sin(n\alpha)}{n}\frac{H_n(kr)}{H_n(ka)}\cos(n\theta), \tag{46}$$

in which the prime after the sum means that the first term is halved.

The related parameters and the used mesh patterns in precious numerical example are retained and the parameter $\alpha = \pi/6$ is used here. Likewise, the imaginary part of the radiated acoustic pressure results at a distance of $R = 1$ m from the center of the cylinder is computed and discussed here. Figure 17 gives the numerical results of the acoustic pressure from different numerical techniques. For comparison, the exact solutions are also plotted in the figures. Since infinite terms are involved in the exact solutions, the infinite series are truncated after a very large number of

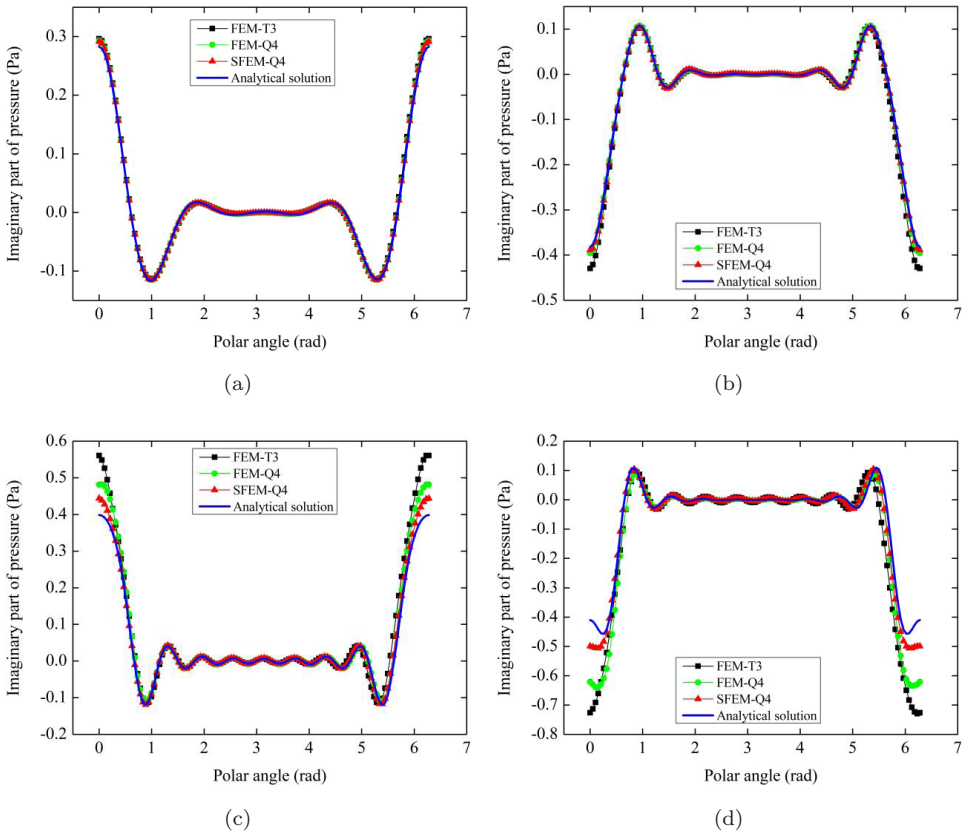


Fig. 17. The imaginary part of the radiated acoustic pressure results from a portion of the infinite cylinder for different non-dimensional wave number values: (a) $ka = 3$; (b) $ka = 6$; (c) $ka = 9$; (d) $ka = 12$.

terms and then the sufficient small truncation error is ensured. To clearly analyze and discuss the accuracy of the numerical results, four different non-dimensional wave numbers ($ka = 3, 6, 9$ and 12) are used in this numerical example. From the figures, it is obvious that all the numerical results have similar accuracy and are in good agreement with the exact solutions at low wave number range. As the wave number increases, the present SFEM-Q4 will exhibit outstanding behaviors and the accuracy of the obtained results obviously surpass the FEM-Q4 and FEM-T3. From these findings, it is demonstrated that the present SFEM-Q4 can achieve more accurate results than the original FEM-Q4 and is capable of solving more complicated acoustic radiation problems, especially in large wave number range.

### 6.3. *The acoustic radiation from a submarine-like body*

We now consider a more complicated and realistic problem. The model is described in Fig. 18, a submarine-shaped radiator is immersed in water (acoustic wave speed $c = 1500\,\mathrm{m/s}$ and density $\rho = 1000\,\mathrm{kg/m^3}$). Note that the radiated noise from the submarine is mainly from the vibration of the operating engine, a Neumann boundary condition with $v = 10^{-4}\,\mathrm{m/s}$ is prescribed at the stern of the submarine. The artificial boundary is still a circle and the observation point A (see Fig. 19) at a distance of $R = 5\,\mathrm{m}$ from the center of the artificial boundary has a polar angle $\theta = \pi/2$. The involved problem domain is divided into 2,146 elements and

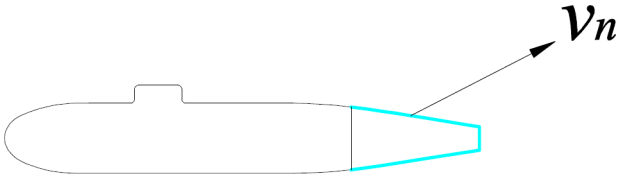


Fig. 18. The radiator with a submarine-like shape.

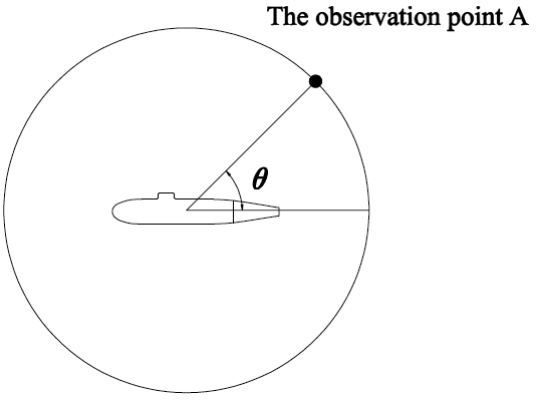


Fig. 19. The illustration of the artificial boundary and the observation point.

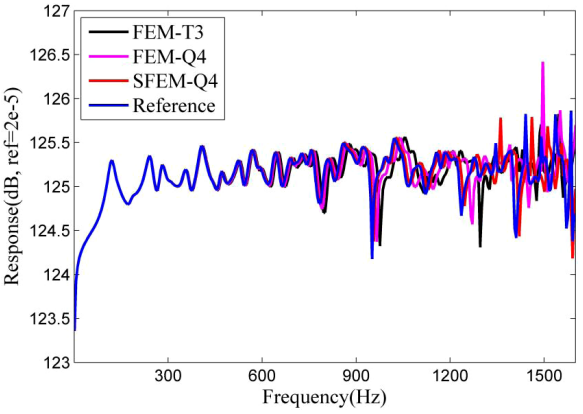


Fig. 20. The direct frequency response results at the observation point from the different numerical methods.

2,042 nodes. The direct frequency response results from the different numerical methods are studied here. The acoustic pressure results at the observation point A are depicted in Fig. 20. The fully considered frequency range is set from 5 to 1500 Hz and the frequency interval is 5 Hz. Note that the exact solution to this complicated problem is relatively difficult to formulate, the reference solutions from a very fine mesh are also presented in the figure. As shown in the figure, for low frequency range, all the numerical results from the three numerical methods agree well with the reference solutions. With the increase of the frequency values, the present SFEM-Q4 will distinguish from the FEM-Q4 and FEM-T3, and can provide more accurate results. From this realistic problem, it is again verified that the SFEM-Q4 works well for acoustic radiation problems and behaves better than the original FEM for complicated problems, especially in high frequency range.

## 7. Conclusions

In this work, a SFEM-Q4 is employed to handle the underwater acoustic radiation problems. From several typical numerical examples, the following conclusions can be obtained.

(1) Due to gradient smoothing operations, the acoustical stiffness matrix obtained from the present SFEM-Q4 behaves softer than that from the original FEM-Q4 and the SFEM-Q4 results are significantly more accurate than the FEM-Q4 and FEM-T3 results for acoustic radiation problems if the identical node distributions are used.
(2) In the process of performing the numerical integration, the traditional mapping and coordinate transformation program have been bypassed successfully, hence the present SFEM-Q4 is less sensitive to the mesh distortion than the original FEM-Q4 and it can work very well for very distorted meshes.

(3) The present SFEM-Q4 has similar behavior as in the FEM-Q4 in controlling the interpolation error and dispersion error for acoustic radiation problems. However, the SFEM-Q4 is more numerically effective to control the numerical error than the FEM-Q4 and FEM-T3 even if a little more computational cost is required for the identical node distributions.
(4) Due to the higher accuracy degree and the faster convergence rate of the present SFEM-Q4, it has great potential in solving more complicated and realistic acoustic radiation problems in the practical engineering applications.



## References

Assaad, J., Decarpigny, J. N., Bruneel, C., Bossut, R. and Hamonic, B. [1993]"Application of the finite element method to two-dimensional radiation problems," *J. Acoust. Soc. Am.* **94**(1), 562–573.

Babuška, I., Ihlenburg, F., Paik, E. T. and Sauter, S. A. [1995] "A generalized finite element method for solving the Helmholtz equation in two dimensions with minimal pollution," *Comput. Methods Appl. Mech. Eng.* **128**(3–4), 325–359.

Belytschko, T., Lu, Y. Y. and Gu, L. [1994] "Element-free Galerkin methods,"*Int. J. Numer. Methods Eng.* **37**(2), 229–256.

Berenger, J. P. [1994] "A perfectly matched layer for the absorption of electromagnetic waves," *J. Comput. Phys.* **114**(2), 185–200.

Bordas, S. and Natarajan, S. [2010] "On the approximation in the smoothed finite element method (SFEM)," *Int. J. Numer. Methods Eng.* **81**(5), 660–670.

Bordas, S., Natarajan, S., Kerfriden, P., Augarde, C. E., Mahapatra, D. R.,Rabczuk, T. and Pont, S. D. [2011]. "On the performance of strain smoothing for quadratic and enriched finite element approximations (XFEM/GFEM/PUFEM)," *Int. J. Numer. Methods Eng.* **86**(4–5), 637–666.

Bordas, S. P., Rabczuk, T., Hung, N. X., Nguyen, V. P., Natarajan, S., Bog, T. andHiep, N. V. [2010] "Strain smoothing in FEM and XFEM,".*Comput. Struct.***88**(23), 1419–1443.

Bouillard, P. and Suleaub, S. [1998] "Element-free Galerkin solutions for Helmholtz problems: Formulation and numerical assessment of the pollution effect," *Comput. Methods Appl. Mech. Eng.* **162**(1–4), 317–335.

Chai, Y. B., Li, W., Gong, Z. X. and Li, T. Y. [2016a] "Hybrid smoothed finite element method for two-dimensional underwater acoustic scattering problems," *Ocean Eng.* **116**, 129–141.

Chai, Y. B., Li, W., Gong, Z. X. and Li, T. Y. [2016c] "Hybrid smoothed finite element method for two dimensional acoustic radiation problems," *Appl.Acoust.* **103**, 90–101.

Chai, Y. B., Li, W., Li, T. Y. Gong, Z. X. and You, X. Y. [2016b] "Analysis of underwater acoustic scattering problems using stable node-based smoothed finite element method," *Eng. Anal. Bound. Elem.* **72**, 27–41.

Chai, Y. B., Li, W., Liu, G. R., Gong, Z. X. and Li, T. Y. [2017] "Asuperconvergent alpha finite element method (S$\alpha$FEM) for static and free vibration analysis of shell structures," *Comput. Struct.* **179**, 27–47.

Chen, M., Li, M. and Liu, G. R. [2016] "Mathematical basis of G Spaces," *Int. J. Comput. Methods* **13**(4), 1641007.

Chen, L., Rabczuk, T., Bordas, S. P. A., Liu, G. R., Zeng, K. Y. and Kerfriden, P. [2012] "Extended finite element method with edge-based strain smoothing (ESm-XFEM) for linear elastic crack growth," *Comput. Methods Appl. Mech.Eng.* **209**, 250–265.

Chen, W. and Wang, F. [2016] "Singular boundary method using time-dependent fundamental solution for transient diffusion problems," *Eng. Anal. Bound. Elem.* **68**, 115–123.

Chen, W., Zhang, J. Y. and Fu, Z. J. [2014] "Singular boundary method for modified Helmholtz equations," *Eng. Anal. Bound. Elem.* **44**, 112–119.

Cui, X. Y. and Chang, S. [2015] "Edge-based smoothed finite element method using two-step Taylor Galerkin algorithm for lagrangian dynamic problems," *Int. J. Comput. Methods* **12**(5), 1550028.

Cui, X. Y., Chang, S. and Li, G. Y. [2015] "A two-step Taylor Galerkin smoothedfinite element method for Lagrangian dynamic problem," *Int. J. Comput. Methods* **12**(4), 1540004.

Cui, X. Y., Hu, X. B., Li, G. Y. and Liu, G. R. [2016] "A modified smoothed finite element method for static and free vibration analysis of solid mechanics," *Int. J. Comput. Methods* **13**(6), 1650043.

Dai, K. Y. and Liu, G. R. [2007] "Free and forced vibration analysis using the smoothed finite element method (SFEM)," *J. Sound Vib.* **301**(3–5), 803–820.

Deraemaeker, A. Babuska, I. and Bouillard, P. [1999] "Dispersion and pollution of the FEM solution for the Helmholtz equation in one, two and three dimensions," *Int. J. Numer. Methods Eng.* **46**(4), 471–499.

DiPerna, D. T. and Stanton, T. K. [1994] "Sound scattering by cylinders of noncircular cross section: A conformal mapping approach," *J. Acoust. Soc.Am.* **96**(5), 3064–3079.

Feng, H., Cui, X. Y. and Li, G. Y. [2016a] "A stable nodal integration method with strain gradient for static and dynamic analysis of solid mechanics." *Eng. Anal. Bound. Elem.* **62**, 78–92.

Feng, S. Z., Cui, X. Y., Chen, F., Liu, S. Z. and Meng, D. Y. [2016b] "An edge/face-based smoothed radial point interpolation method for static analysis of structures," *Eng. Anal. Bound. Elem.* **68**, 1–10.

Fu, Z. J., Chen, W. and Gu, Y. [2014] "Burton–Miller-type singular boundary method for acoustic radiation and scattering," *J. Sound Vib.* **333**(16), 3776–3793.

Fu, Z. J., Chen, W., Lin, J. and Cheng, A. H. D. [2015] "Singular boundary method for various exterior wave applications," *Int. J. Comput. Methods* **12**(2), 1550011.

Giljohann, D. and Bittner, M. [1998] "The three-dimensional DtN finite element method for radiation problems of the Helmholtz equation," *J. Sound Vib.* **212**(3), 383–394.

Gong, Z. X., Chai, Y. B. and Li, W. [2016a] "Coupled analysis of structural–acoustic problems using the cell-based smoothed three-node mindlin plate element," *Int. J. Comput. Methods* **13**(2), 1640007.

Gong, Z. X., Li, W., Chai, Y. B., Zhao, Y. and Mitri, F. G. [2017] "T-matrix method for acoustical Bessel beam scattering from a rigid finite cylinder with spheroidal endcaps," *Ocean Eng.* **129**, 507–519.

Gong, Z. X., Li, W., Mitri, F. G., Chai, Y. and Zhao, Y. [2016b] "Arbitrary scattering of an acoustical Bessel beam by a rigid spheroid with large aspect-ratio," *J. Sound Vib.* **383**, 233–247.

Harari, I. and Djellouli, R. [2004] "Analytical study of the effect of wave number on the performance of local absorbing boundary conditions for acoustic scattering," *Appl. Numer. Math.* **50**(1), 15–47.

Harari, I. and Hughes, T. J. R. [1992] "Galerkin/least-squares finite element methods for the reduced wave equation with non-reflecting boundary conditions in unbounded domains," *Comput. Methods Appl. Mech. Eng.* **98**(3), 411–454.

He, Z. C., Li, E., Li, G. Y., Wu, F., Liu, G. R. and Nie, X. [2015] "Acoustic simulation using $\alpha$-FEM with a general approach for reducing dispersion error," *Eng. Anal. Bound. Elem.* **61**, 241–253.

He, Z. C., Li, G. Y., Li, E., Zhong, Z. H. and Liu, G. R. [2014] "Mid-frequency acoustic analysis using edge-based smoothed tetrahedron radialpoint interpolation methods," *Int. J. Comput. Methods* **11**(5), 1350103.

He, Z. C., Li, G. Y., Zhong, Z. H., Cheng, A. G., Zhang, G. Y., Li, E. and Liu, G.R. [2012] "An ES-FEM for accurate analysis of 3D mid-frequency acoustics using tetrahedron mesh," *Comput. Struct.* **106–107**, 125–134.

He, Z. C., Liu, G. R., Zhong, Z. H., Wu, S. C., Zhang, G. Y. and Cheng, A. G.[2009] "An edge-based smoothed finite element method (ES-FEM) for analyzing three-dimensional acoustic problems," *Comput. Methods Appl. Mech. Eng.* **199**(1–4), 20–33.

Hu, X. B., Cui, X. Y., Feng, H. and Li, G. Y. [2016] "Stochastic analysis using the generalized perturbation stable node-based smoothed finite element method," *Eng. Anal. Bound. Elem.* **70**, 40–55.

Hu, X., Cui, X., Zhang, Q., Wang, G. and Li, G. [2017] "The stable node-based smoothed finite element method for analyzing acoustic radiation problems," *Eng. Anal. Bound. Elem.* **80**, 142–151.

Ihlenburg, F. and Babuška, I. [1995a] "Dispersion analysis and error estimation of Galerkin finite element methods for the Helmholtz equation," *Int. J. Numer. Methods Eng.* **38**(22), 3745–3774.

Ihlenburg, F. and Babuška, I. [1995b] "Finite element solution of the Helmholtz equation with high wave number Part I: The $h$-version of the FEM," *Comput. Math. Appl.* **30**(9), 9–37.

Ihlenburg, F. and Babuška, I. [1997] "Finite element solution of the Helmholtz equation with high wave number Part II: The hp version of the FEM,"*SIAM J. Numer. Anal.* **34**(1), 315–358.

Ihlenburg, F., Babuška, I. and Sauter, S. [1997] "Reliability of finite element methods for the numerical computation of waves," *Adv. Eng. Softw.* **28**(7), 417–424.

Jiang, C., Zhang, Z. Q., Liu, G. R., Han, X. and Zeng, W. [2015] "An edge-based/node-based selective smoothed finite element method using tetrahedrons for cardiovascular tissues," *Eng. Anal. Bound. Elem.* **59**, 62–77.

Keller, J. B. and Givoli, D. [1989] "Exact non-reflecting boundary conditions,"*J. Comput. Phys.* **82**(1), 172–192.

Kim, D., Kim, J. and Sheen, D. [1996] "Absorbing boundary conditions for wave propagation in viscoelastic media," *J. Comput. Appl. Math.* **76**(1–2), 301–314.

Li, J. P., Chen, W., Fu, Z. J. and Sun, L. L. [2016a] "Explicit empirical formula evaluating original intensity factors of singular boundary method for potential and Helmholtz problems," *Eng. Anal. Bound. Elem.* **73**, 161–169.

Li, W., Chai, Y. B., Lei, M. and Li, T. Y. [2017a] "Numerical investigation ofthe edge-based gradient smoothing technique for exterior Helmholtz equation in two dimensions," *Comput. Struct.* **182**, 149–164.

Li, W., Chai, Y. B., Lei, M. and Liu, G. R. [2014] "Analysis of coupled structural-acoustic problems based on the smoothed finite element method (S-FEM)," *Eng. Anal. Bound. Elem.* **42**, 84–91.

Li, W., Gong, Z. X., Chai, Y. B., Cheng, C., Li, T. Y., Zhang, Q. F. and Wang, M. S. [2017b] "Hybrid gradient smoothing technique with discrete shear gap methodfor shell structures," *Comput. Math. Appl.*, http://dx.doi.org/10.1016/j.camwa.2017.06.047.

Li, W., You, X. Y., Chai, Y. B. and Li, T. Y. [2016b] "Edge-based smoothed three-node mindlin plate element" *J. Eng. Mech.* **142**(9), 04016055.

Liu, G. R. [2009] "On G space theory," *Int. J. Comput. Methods* **6**(2), 257–289.

Liu, G. R. [2016]. "An overview on meshfree methods: For computational solid mechanics," *Int. J. Comput. Methods* **13**(5), 1630001.

Liu, G. R., Chen, M. and Li, M. [2017] "Lower bound of vibration modes using the node-based smoothed finite element method (NS-FEM)," *Int. J. Comput. Methods* **14**(4), 1750036.

Liu, G. R., Dai, K. Y. and Nguyen-Thoi, T. [2007a] "A smoothed finite element method for mechanics problems," *Comput. Mech.* **39**(6), 859–877.

Liu, G. R., Nguyen-Thoi, T., Dai, K. Y. and Lam, K. Y. [2007b] "Theoretical aspects of the smoothed finite element method (SFEM)," *Int. J. Numer. Methods Eng.* **71**(8), 902–930.

Liu, G. R. and Zhang, G. Y. [2013] *Smoothed Point Interpolation Methods: G Space Theory and Weakened Weak Forms* (World Scientific, Singapore).

Liu, G. R., Zeng, W. and Nguyen-Xuan, H. [2013] "Generalized stochastic cell-based smoothed finite element method (GS_CS-FEM) for solid mechanics," *Finite Elem. Anal. Des.* **63**, 51–61.

Nguyen, V. P., Rabczuk, T., Bordas, S. and Duflot, M. [2008] "Meshless methods: A review and computer implementation aspects," *Math. Comput. Simulation* **79**, 763–813.

Nguyen-Thanh, N., Rabczuk, T., Nguyen-Xuan, H. and Bordas, S. [2008] "A smoothed finite element method for shell analysis," *Comput. Methods Appl. Mech. Eng.* **198**(2), 165–177.

Nguyen-Thanh, N., Rabczuk, T., Nguyen-Xuan, H. and Bordas, S. [2011] "An alternative alpha finite element method with discrete shear gap technique for analysis of isotropic Mindlin–Reissner plates," *Finite Elem. Anal. Des.* **47**(5), 519–535.

Nguyen-Thoi, T., Phung-Van, P., Rabczuk, T., Nguyen-Xuan, H. and Le-Van, C. [2013]"An application of the ES-FEM in solid domain for dynamic analysis of 2D fluid–solid interaction problems," *Int. J. Comput. Methods* **10**(1),1340003.

Nguyen-Thoi, T., Rabczuk, T., Ho-Huu, V., Le-Anh, L., Dang-Trung, H. and Vo-Duy, T. [2017] "An extended cell-based smoothed three-node Mindlin plate element (XCS-MIN3) for free vibration analysis of cracked FGM plates," *Int. J.Comput. Methods* **14**(2), 1750011.

Nguyen-Thoi, T., Rabczuk, T., Lam-Phat, T., Ho-Huu, V. and Phung-Van, P. [2014]"Free vibration analysis of cracked Mindlin plate using an extended cell-based smoothed discrete shear gap method (XCS-DSG3)," *Theor. Appl. Fract. Mech.* **72**, 150–163.

Nguyen-Thoi, T., Vu-Do, H. C., Rabczuk, T. and Nguyen-Xuan, H. [2010] "Anode-based smoothed finite element method (NS-FEM) for upper bound solution toviscoelastoplastic analyses of solids using triangular and tetrahedral meshes," *Comput. Methods Appl. Mech. Eng.* **199**(45), 3005–3027.

Nguyen-Xuan, H., Bordas, S. and Nguyen-Dang, H. [2008a] "Smooth finite element methods: Convergence, accuracy and properties," *Int. J. Numer. Methods Eng.* **74**(2), 175–208.

Nguyen-Xuan, H., Liu, G. R., Bordas, S., Natarajan, S. and Rabczuk, T. [2013] "An adaptive singular ES-FEM for mechanics problems with singular field of arbitrary order," *Comput. Methods Appl. Mech. Eng.* **253**, 252–273.

Nguyen-Xuan, H., Rabczuk, T., Bordas, S. and Debongnie, J. F. [2008b] "A smoothed finite element method for plate analysis," *Comput. Methods Appl. Mech. Eng.* **197**(13), 1184–1203.

Nguyen-Xuan, H., Rabczuk, T., Nguyen-Thanh, N., Nguyen-Thoi, T. and Bordas, S. [2010] "A node-based smoothed finite element method with stabilized discrete shear gap technique for analysis of Reissner–Mindlin plates," *Comput. Mech.* **46**(5), 679–701.

Seybert, A. F., Soenarko, B., Rizzo, F. J. and Shippy, D. J. [1986] "A special integral equation formulation for acoustic radiation and scattering for axisymmetric bodies and boundary conditions," *J. Acoust. Soc. Am.* 80(4),1241–1247.

Seybert, A. F., Wu, T. W. and Wu, X. F. [1988] "Radiation and scattering of acoustic waves from elastic solids and shells using the boundary element method," *J. Acoust. Soc. Am.* **84**(5), 1906–1912.

Stewart, J. R. and Hughes, T. J. R. [1996] "*A posteriori* error estimation and adaptive finite element computation of the Helmholtz equation in exterior domains," *Finite Elem. Anal. Des.* **22**(1), 15–24.

Thompson, L. L. [2006] "A review of finite-element methods for time-harmonic acoustics," *J. Acoust. Soc. Am.* **119**(3), 1315–1330.

Vu-Bac, N., Nguyen-Xuan, H., Chen, L., Bordas, S., Kerfriden, P., Simpson, R. N., Liu, G. R. and Rabczuk, T. [2011] "A node-based smoothed extended finite element method (NS-XFEM) for fracture analysis," *Comput. Model. Eng. Sci.* **73**(4), 331–355.

Vu-Bac, N., Nguyen-Xuan, H., Chen, L., Lee, C. K., Zi, G., Zhuang, X., Liu, G. R. and Rabczuk, T. [2013] "A phantom-node method with edge-based strain smoothing for linear elastic fracture mechanics," *J. Appl. Math.* **2013**, 978026.

Wan, D. T., Hu, D., Yang, G. and Long, T. [2016] "A fully smoothed finite element method for analysis of axisymmetric problem," *Eng. Anal. Bound. Elem.* **72**, 78–88.

Wang, G., Cui, X. Y., Feng, H. and Li, G. Y. [2015a] "A stable node-based smoothed finite element method for acoustic problems," *Comput. Methods Appl. Mech.Eng.* **297**, 348–370.

Wang, G., Cui, X. Y. and Li, G. Y. [2016] "An element decomposition method for the Helmholtz equation," *Commun. Comput. Phys.* **20**(5), 1258–1282.

Wang, G., Cui, X. Y., Liang, Z. M. and Li, G. Y. [2015b] "A coupled smoothed finite element method (S-FEM) for structural-acoustic analysis of shells," *Eng. Anal. Bound. Elem.* **61**, 207–217.

Wenterodt, C. and von Estorff, O. [2009] "Dispersion analysis of the meshfree radial point interpolation method for the Helmholtz equation," *Int. J. Numer. Methods Eng.* **77**(12), 1670–1689.

Wu, F., Yao, L. Y., Hu, M. and He, Z. C. [2017] "A stochastic perturbationedge-based smoothed finite element method for the analysis of uncertain structural-acoustics problems with random variables," *Eng. Anal. Bound. Elem.* **80**, 116–126.

Wu, G., Zhang, J., Li, Y., Yin, L. and Liu, Z. [2016] "Analysis of transient thermo-elastic problems using a cell-based smoothed radial point interpolation method," *Int. J. Comput. Methods* **13**(5), 1650023.

Xu, X., Zheng, Z. Q., Gu, Y. T. and Liu, G. R. [2016] "A quasi-conforming point interpolation method (QC-PIM) for elasticity problems," *Int. J. Comput. Methods* **13**(5), 1650026.

Xue, B. Y., Wu, S. C., Zhang, W. H. and Liu, G. R. [2013] "A smoothed FEM (S-FEM)for heat transfer problems," *Int. J. Comput. Methods* **10**(1), 1340001.

Yang, Y. T., Zheng, H. and Du, X. L. [2016] "An enriched edge-based smoothed FEM for linear elastic fracture problems," *Int. J. Comput. Methods* **14**(5), 1750052.

Yao, L., Li, Y. and Li, L. [2016] "Dispersion error reduction for acoustic problems using the smoothed finite element method (SFEM)," *Int. J. Numer. Meth. Fluids* **80**(6), 343–357.

Yao, L. Y., Yu, D. J., Cui, X. Y. and Zang, X. G. [2010] "Numerical treatment of acoustic problems with the smoothed finite element method," *Appl. Acoust.* **71**(8), 743–753.

Zeng, W. and Liu, G. R. [2016] "Smoothed finite element methods (S-FEM): An overview and recent developments," *Arch. Comput. Method Eng.* 1–39.

Zeng, W., Liu, G. R., Jiang, C., Nguyen-Thoi, T. and Jiang, Y. [2016] "A generalized beta finite element method with coupled smoothing techniques for solid mechanics," *Eng. Anal. Bound. Elem.* **73**, 103–119.

Zhang, G. Y., Li, Y., Gao, X. X., Hui, D., Wang, S. Q. and Zong, Z. [2015] "Smoothed point interpolation method for elastoplastic analysis," *Int. J. Comput. Methods* **12**(4), 1540013.

Zhang, G. Y., Li, Y., Wang, H. and Zong, Z. [2016] "A linear complementarity formulation of meshfree method for elastoplastic analysis of gradient-dependent plasticity," *Eng. Anal. Bound. Elem.* **73**, 1–13.

Zienkiewicz, O. C. [2000] "Achievements and some unsolved problems of finite element method," *Int. J. Numer. Methods Eng.* **47**(1–3), 8–28.